Performance Analysis of Grid-Connected Wind Turbine System Under Inter-Turn Short-Circuit Fault Conditions

T. Sellami[1,2], H. Berriri[1], S. Jelassi[2], A. M Darcherif[2] and M.F. Mimouni[1]

[1]Electrical Department, National Engineering School of Monastir, Monastir 5000, Tunisia

[2] ECAM-EPMI, Graduate School of Engineering, 95000 Cergy, France

(sellami.takwa8@gmail.com, hanenberriri@yahoo.fr, s.jelassi@ecam-epmi.fr, m.darcherif@ecam-epmi.fr, MFaouzi.Mimouni@enim.rnu.tn)

[‡] Corresponding Author; Takwa Sellami, ESIER, Electrical Department, ENIM, Monastir 5000, Tunisia and Quartz-Lab, EA 9373, Engineering Department, Cergy-Pontoise University, Cergy 95000, France. Tel: +33 061 105 2053,

sellami.takwa8@gmail.com

Received: 11.07.2017 Accepted: 20.08.2017

Abstract- This paper aims to analyze the performance of a variable-speed wind turbine system under internal faulty conditions. Thus, a wind turbine grid-connected system driven three-phase induction generator is modeled. The turbine mathematical model controlled by Maximum Power Point Tracking (MPPT) method is presented. The mathematical model of the Induction Generator (IG) is also set up in the (*abc*)-reference frame. Indirect Rotor Flux Oriented Control (IRFOC) technique is developed to control the IG. Afterwards, Inter-Turn Short-Circuit (ITSC) fault affecting the stator windings of the system IG is investigated. Different severity cases of the ITSC fault are considered in order to assess the fault impact on the system continuity of service and the quality of the supplied power to the grid signal. The ITSC fault effects on the turbine, the generator and the stator-side converter are discussed. Simulations, realized under MATLAB/SIMULINK below both healthy and faulty conditions, highlight the system requirement of a quick detection algorithm sensitive to short-circuit fault.

Keywords Wind turbine grid-connected system, inter-turn short-circuit fault, maximum power Point tracking, indirect Rotor flux oriented control.

1. Introduction

Renewable energies are still worthy and trusty solutions for environmental degradation conditions. The wind presents one of the most essential sources of renewable energies. Thus, modeling, control and diagnosis of wind turbine systems are important issues [1]. Many authors studied wind turbine systems modelling and control techniques. Diagnosis strategies are also important tasks for ensuring reliability and nonstop service of systems. Nevertheless, analyzing the performances of control methods under faulty conditions is the most challenging task. Hence, fault tolerant control methods are required to ensure the continuity of service under faulty conditions and to protect the system equipment [2].

Wind turbine system diagnosis concerns especially the generator. Many faults can affect the generator like rotor or stator broken bars, eccentricities and windings short-circuits. Stator windings faults are serious faults because they progress quickly in machines. In fact, they can quickly destroy the machine, affect the converters and the transformer and stop the wind turbine system. Inter-Turn Short-Circuit (ITSC) fault can easily lead to turn-turn or turn-ground short-circuit. This fault is generally engendered by mechanical stress or partial discharge [3].

To avoid this stator fault effects, effective detection algorithms have to be implemented. Many authors studied short-circuit fault-detection methods [4]. Motor current and speed signatures are mainly analyzed in most fault-detection methods. In fact, stator currents spectra contain important information about short-circuit fault permitting its isolation without stopping the service.

Three-phase Induction Generator (IG) drives are usually used in variable-speed wind turbine systems because they are robust, not expensive and easily maintained machines [5]. Indirect Rotor Flux Oriented Control (IRFOC) is typically used to control the machine by imposing its rotor flux. IRFOC is the most adapted control method as it excludes the leakage reactance influence of both the stator and the rotor. However, the efficacy of this control method is not tested yet for variable-speed turbines under ITSC fault presence [6].

Wind turbine systems modelling is developed in the second section. Thus, the model of controlled turbine via Maximum Power Point Tracking (MPPT) method is established. IRFOC controlling the IG model is also established in the (*abc*)-reference frame. In the third section, ITSC fault is investigated. Then, simulation results are discussed under both healthy and faulty conditions in the fourth section. A comparison is made under healthy and ITSC faulty conditions to highlight the fault impact on the system. In the last section, conclusions are presented.

2. Wind Turbine System Modelling

Wind turbine driven induction generator transforms wind energy to electrical one. Produced energy is delivered to the grid through converters and transformers.

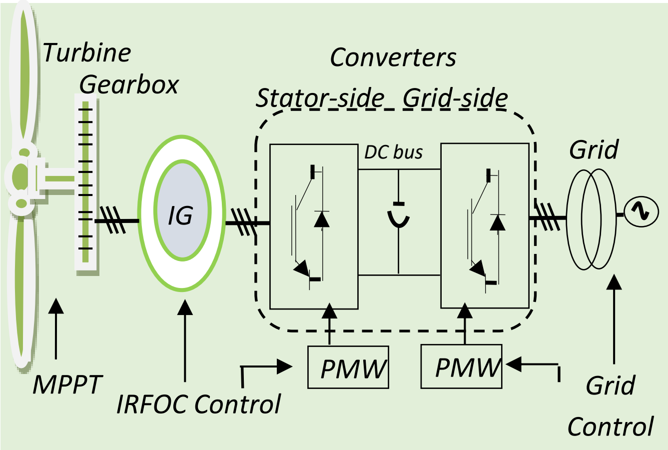

Fig. 1. Wind turbine driven IG closed loop system.

The two converters (stator-side converter and grid-side converter) connected by a DC bus voltage, ensure decoupling electrical frequency to mechanical one. A transformer is required to adapt the grid voltage. Variable-speed turbine driven IG, as sketched in Fig. 1, is basically composed of a turbine and a generator. To adapt the turbine speed to electrical frequency, a gearbox is required. However, control algorithms are required to control the system. The turbine is controlled by MPPT method [7-8]. The IG in this study is controlled by IRFOC method [9]. IRFOC technique controls the stator-side converter through feeding its Pulse Width-Modulated (PWM) by three-phase voltages reference. A DC bus voltage connects the two converters. Controlling the power injected to the grid is also needed based on a grid control algorithm. The grid control technique controls the grid-side converter through feeding its PWM by three-phase voltages reference. For both IRFOC and power control synthesis, transformation from (*abc*)-reference frame to (*dq*)-Park frame are required [10].

2.1 Turbine model

The mechanical part the turbine is composed of *n* orientable blades. According to the wind speed *V*, the blades are fixed to a rotating drive shaft at a speed $\Omega_{turbine}$. An equivalent mechanical model of the wind turbine system is presented in Fig. 2. The turbine, characterized by an inertia $J_{turbine}$, is connected to a generator. The generator transforms the mechanical energy to electrical one. The rotor of the generator is characterized by an inertia J_g and coefficient of friction relative to the shaft *f*. A gearbox is required in some turbines to increase the rotor speed Ω_{mec} through a multiplication by a coefficient *G*. The turbine absorbs a wind torque C_{ar}. Then, the turbine rotor and the gearbox transmit a torque C_g to the generator. The generator rotating at the speed Ω_{mec}, produces an electromagnetic torque C_{em}.

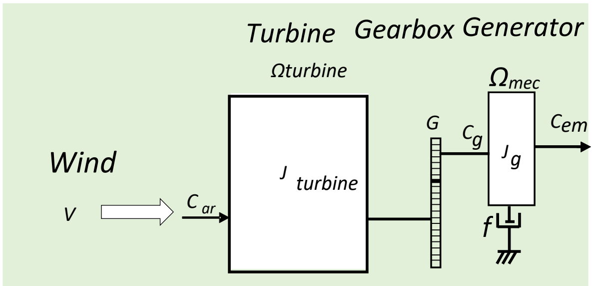

Fig. 2 Equivalent mechanical system of the wind turbine.

The turbine total inertia J_t can be defined by:

$$J_t = \frac{J_{turbine}}{G^2} + J_g \qquad (1)$$

The mechanical equation of the turbine is defined by:

$$J_t \frac{d\Omega_{mec}}{dt} = C_{em} - C_g - f\Omega_{mec} \qquad (2)$$

The torque C_g is defined by:

$$C_g = \frac{C_{ar}}{G} = \frac{1}{G}\frac{P_{ar}}{\Omega_{mec}} = \frac{1}{G\Omega_{mec}}\frac{1}{2}\rho\,\pi R^2 V^3 C_p(\lambda,\beta) \qquad (3)$$

Where *R* is the rotor radius of the turbine, ρ is the air density depending of the air temperature and the altitude. C_p is the power coefficient defined as a function of the pitch angle β and the tip speed ratio λ defined by:

$$\lambda = \frac{R\Omega_{mec}}{V} \qquad (4)$$

2.2 Maximum Power Point Tracking (MPPT) control

A maximum theoretical value of C_p indicated by the Betz limit assumes that C_{p_max} = 16/27 = 0.593.By measuring the generator rated powers at different speeds, the variation of C_p can be determined. Pitch angel and MPPT control methods are used in order to extract the maximum power from the turbine using PI controllers. MPPT loop, as presented in Fig. 3, is based on controlling the rotor speed in order to maintain the turbine tip ratio λ at its maximum value [11]. The maximum value of λ called λ_{opt}, ensures a maximum turbine power coefficient C_{p_max} guaranteeing a maximum produced power by the turbine.

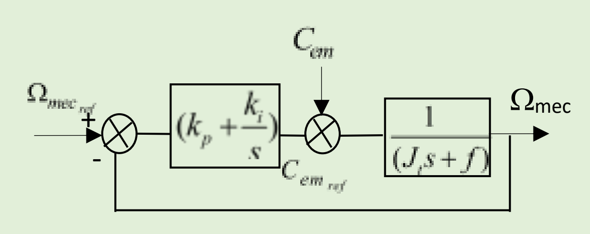

Fig. 3. Control structure of the turbine speed.

The turbine speed reference calculated by the conventional MPPT is expressed by:

$$\Omega_{mec_{ref}} = \frac{V\lambda_{opt}}{R} \quad (5)$$

The rotational speed reference has to be then adjusted so that the turbine can be subjected to the current tidal velocity, produces its maximum power. The turbine torque reference is then expressed by:

$$C_{em_{ref}} = \frac{V\lambda_{opt}}{R}\frac{1}{2}\rho\,\pi R^2\,V^3 C_{p\max} \quad (6)$$

Using Laplace Transformation and neglecting C_g the mechanical equation becomes:

$$\Omega_{mec} = \frac{C_{em}}{(J_t s + f)} \quad (7)$$

The turbine is controlled by a PI controller as shown in Fig. 3. The PI corrector function is expressed by:

$$C(s) = k_p + \frac{k_i}{s} \quad (8)$$

Where K_p is the corrector proportional parameter of the controller adjusting the system reply time. K_i is the integral parameter reducing the overtaking. The parameters values are fixed according to required performances by imposing ω_0 is the angular natural frequency of the closed loop system and ξ is damping factor of the closed loop system [12-13]

2.3 *Induction generator model*

In order to study inter-turn short-circuit fault, it is obligatory to develop the IG model in the natural reference frame (*abc*). Park transformation cannot be used because of the imbalance of the system currents and voltages caused by the fault [14]. The equivalent circuit of three-phase IG is described in Fig. 4. s_1, s_2, and s_3 are the three identique phases of the stator. Each phase has a stator phase resistance r^s. L^s presents the phase self-inductance. The neutral is connected ($V_{NN'}$=0V). For the rotor scheme, three phases are also presented. Each one is characterized by a rotor phase resistance r^r and a self-inductance L^r. M^s and M^r present respectively the stator mutual inductances and the rotor mutual inductance. M_{sr} is the mutual inductance between stator and rotor phases. J_g presents the moment inertia of the generator. p is the machine number of pole pair's. Ω_{mec} is the mechanical angular speed of the machine.

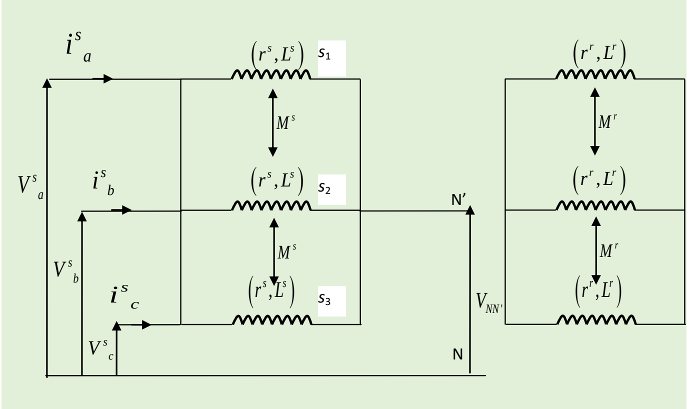

Fig. 4. Equivalent circuit of the induction generator.

The IG system is modeled in (*abc*)-reference frame by voltage and currents vector (V^s_{abc}, $V_{abc}{}^r$, i^s_{abc}, i^r_{abc} and i_{abc}) defined by:

$$[V^s{}_{abc}] = \left[V^s{}_a \;\; V^s{}_b \;\; V^s{}_c\right]^T ; [V^r{}_{abc}] = \left[V^r{}_a \;\; V^r{}_b \;\; V^r{}_c\right]^T$$

$$[i^s{}_{abc}] = \left[i^s{}_a \;\; i^s{}_b \;\; i^s{}_c\right]^T ; [i^r{}_{abc}] = \left[i^r{}_a \;\; i^r{}_b \;\; i^r{}_c\right]^T$$

$$[i_{abc}] = \left[i^s{}_a \;\; i^s{}_b \;\; i^s{}_c \;\; i^r{}_a \;\; i^r{}_b \;\; i^r{}_c\right]^T$$

IG voltage equations developed in the natural reference frame (*abc*) are expressed by:

$$\begin{cases} \left[V^s{}_{abc}\right] = \left[R^s{}_{abc}\right]\left[i^s{}_{abc}\right] + \left[L^{ss}{}_{abc}\right]\frac{d}{dt}\left[i^s{}_{abc}\right] + \frac{d}{dt}(\left[M^{sr}{}_{abc}\right]\left[i^r{}_{abc}\right]) \\ \left[V^r{}_{abc}\right] = [0] = \left[R^r{}_{abc}\right]\left[i^r{}_{abc}\right] + \left[L^{rr}{}_{abc}\right]\frac{d}{dt}\left[i^r{}_{abc}\right] + \frac{d}{dt}(\left[M^{rs}{}_{abc}\right]\left[i^s{}_{abc}\right]) \end{cases} \quad (9)$$

Where the resistance matrices $[R^s{}_{abc}]$ and $[R^r{}_{abc}]$ are expressed by:

$$\left[R^s{}_{abc}\right] = \begin{bmatrix} r^s & 0 & 0 \\ 0 & r^s & 0 \\ 0 & 0 & r^s \end{bmatrix} \quad \left[R^r{}_{abc}\right] = \begin{bmatrix} r^r & 0 & 0 \\ 0 & r^r & 0 \\ 0 & 0 & r^r \end{bmatrix}$$

The stator and rotor mutual inductance matrices $[L^{ss}{}_{abc}]$and $[L^{rr}{}_{abc}]$ are expressed by:

$$\left[L^{ss}{}_{abc}\right] = \begin{bmatrix} L^s + l^s & M^s & M^s \\ M^s & L^s + l^s & M^s \\ M^s & M^s & L^s + l^s \end{bmatrix}$$

$$\left[L^{rr}{}_{abc}\right]=\begin{bmatrix} L^r+l^r & M^r & M^r \\ M^r & L^r+l^r & M^r \\ M^r & M^r & L^r+l^r \end{bmatrix}$$

The stator and rotor mutual inductance interaction matrix $[M^{sr}(\theta)]$ is expressed by:

$$\left[M^{sr}(\theta)\right]=M_{sr}\begin{bmatrix} \cos(\theta) & \cos(\theta+\frac{2\pi}{3}) & \cos(\theta+\frac{4\pi}{3}) \\ \cos(\theta+\frac{4\pi}{3}) & \cos(\theta) & \cos(\theta+\frac{2\pi}{3}) \\ \cos(\theta+\frac{2\pi}{3}) & \cos(\theta+\frac{4\pi}{3}) & \cos(\theta) \end{bmatrix}$$

The produced electromagnetic torque C_{em} is given by:

$$Cem=(\frac{1}{2})p\left[i_{abc}\right]^T\frac{d\left[L_{abc}\right]}{d\theta}\left[i_{abc}\right] \tag{10}$$

2.4 Induction generator modelling in (d,q)-Park reference frame for IRFOC control technique

The establishing of the IG model in Park reference frame (d,q), following d (direct axis) and q (quadrature axis), is required in order to control the machine. Basing on Par k rotating transformation matrix. θ_p is the rotating rotor vector angle relatively to the stator. θ is the rotating vector angle relatively to the stator (synchronous speed) ($\theta_r=\theta_p-\theta$)). The ω_p, ω_s and ω are respectively calculated basing on the angles θ_p, θ_s and θ derivating. Ω_{mec} is the mechanical speed. The electric speed is defined by $\omega_r=p\Omega_{\text{mec}}$.

Applying transformation Park, the system becomes:

$$\begin{cases} V^s{}_d=r^s i^s{}_d+\dfrac{d\varphi^s{}_d}{dt}-\omega_p\varphi^s{}_q \\ V^s{}_q=r^s i_{sq}+\dfrac{d\varphi^s{}_q}{dt}+\omega_p\varphi^s{}_d \\ 0=r^r i^r{}_d+\dfrac{d\varphi^r{}_d}{dt}-\left(\omega_p-\omega\right)\varphi^r{}_q \\ 0=r^r i^r{}_q+\dfrac{d\varphi^r{}_q}{dt}+\left(\omega_p-\omega\right)\varphi^r{}_d \end{cases} \tag{11}$$

Where the rotor flux and stator currents in the rotating frame (d,q) are defined by:

$$\begin{cases} \varphi^s{}_d=L_s i^s{}_d+Mi^r{}_d \\ \varphi^s{}_q=L_s i^s{}_q+Mi^r{}_q \\ \varphi^r{}_d=L_r i^r{}_d+Mi^s{}_d \\ \varphi^r{}_q=L_r i^r{}_q+Mi^s{}_q \end{cases} \tag{12}$$

The electromagnetic torque is expressed by:

$$C_{em}=p\frac{M}{L_r}\left(\varphi^s{}_d i^s{}_q-\varphi^s{}_q i^s{}_d\right) \tag{13}$$

It is important to note that Park transformation generates new parameters of the machine calculated from the machine parameters defined in the (abc)-reference frame. New parameters of the stator and rotor are given by [3]:

$L_s=L^s+l^s-M^s$, $L_r=L^r+l^r-M^r$, $M=\frac{3}{2}M_{sr}$, $\tau_s=\frac{L_s}{r^s}$, $\tau_r=\frac{L_r}{r^r}$, $\sigma=1-\frac{M_{sr}{}^2}{L_sL_r}$.

2.5 Indirect Rotor Flux Oriented Control (IRFOC) of induction machine

Indirect Rotor Flux Oriented Control (IRFOC) method principle is to orient the rotor flux according to the d-axis by imposing [3]:

$$\begin{cases} \varphi^r{}_d=\varphi_r \\ \varphi^r{}_q=0 \end{cases} \tag{14}$$

Controlling d and q stator current components ensures an independent control of both decoupled rotor flux and torque. IRFOC is the most adapted control method as it excludes the leakage reactance influence of both the stator and the rotor.

Imposing $\varphi^r{}_q=0$ and using Laplace transformation, the decoupling equations become:

$$\begin{cases} V^s{}_d=(r^s+s\sigma L_s)i^s{}_d+s\dfrac{M}{L_r}\varphi_r-\omega_s\sigma L_s i^s{}_q \\ V^s{}_q=(r^s+s\sigma L_s)i^s{}_q+\omega_s\dfrac{M}{L_r}\varphi_r+\omega_s\sigma L_s i^s{}_d \end{cases} \tag{15}$$

Developing the previous equations, the system equations become:

$$\begin{cases} \varphi_r=\dfrac{M}{1+\tau_r}i^s{}_d \\ C_{em}=p\dfrac{M}{L_r}i^s{}_q \\ \omega_r=\dfrac{M}{\tau_r\varphi_r}i^s{}_q \\ \omega_s=p\Omega-\omega_r \end{cases} \tag{16}$$

The speed control loop is realized based on the MPPT requirements (Fig. 3). IRFOC is based on controlling the flux and stator currents through PI controllers as presented in Fig. 5. The output of the speed controller is the electromagnetic torque reference. The output of the current $i^s{}_d$ controller is the reference voltage $V^s{}_d{}^*$. The output of the current $i^s{}_q$ controller is the reference voltage $V^s{}_q{}^*$. The reference current $i^s{}_d{}^*$ is calculated based on imposed flux φ_r. The PI controllers' parameters of speed, flux and currents controllers are fixed basing on the performances requirements of system (imposed damping ratio and natural frequency) using division compensation technique.

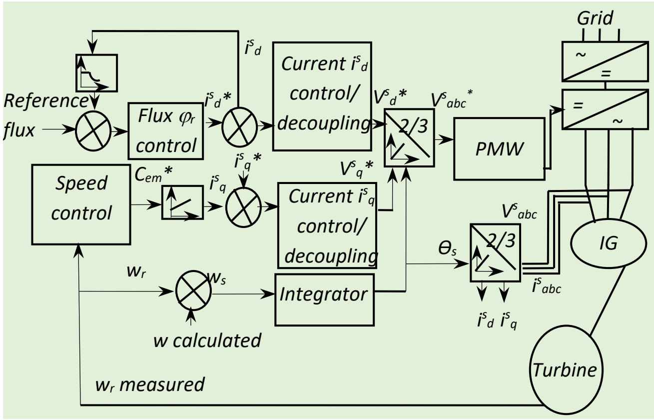

Fig. 5. IRFOC strategy for the induction generator.

IRFOC technique controls the stator-side converter through feeding the Pulse Width-Modulated (PWM) by three-phase voltage reference $V^s_{abc}{}^*$. After achieving the grid-control technique, a power P will finally be injected to the grid.

3. Wind Turbine Genrator Modelling Under Faulty Conditions (ITSC Fault)

Inter-turn short-circuit fault causes an insulation failure in the machine phase windings. In fact, an insulation resistance r_f appears [15]. A current i_f circulates in the resistance r_f. The insulation resistance r_f controls the ITSC fault severity. A severe ITSC fault is defined by a low insulation resistance r_f (toward zero). Unluckily, r_f decreases quickly in most materials [16].

Fig. 6 shows the stator windings model under ITSC fault conditions. The short-circuit occurred in the first phase s_1 .s_1 is characterized by turns phase number N^s. as_1 presents the sub-winding healthy portion of the phase windings s_1. bs_1 presents the sub-winding faulty portion. N^s_f presents the number of short-circuited turns. An ITSC factor k_{cc} is then defined between 0 and 1 ($k_{cc} = N^s_f / N^s$). $M_{1a,2}$ and $M_{1a,3}$ are the mutual inductances between as_1 and respectively the windings s_2 and s_3. $M_{1a,1b}$, $M_{1b,2}$ and $M_{1b,3}$ are respectively created mutual inductances between bs_1 and respectively the windings as_1, s_2 and s_3. M_{sr1}, M_{sr2} are created mutual inductances between respectively as_1, bs_1 and rotor. The stator resistances is also affected by the fault. r^s_{1b} and L^s_{1b} are considered as respectively resistance and self-inductance of faulty winding [18].

It has been admitted in literature [17] that:

$$\begin{cases} L_{1a}+l_{1a}+2M_{1a,1b}+L_{1b}+l_{1b}=L^s+l^s=L_s \\ L_r=L^r+l^r \\ M_{sr1}+M_{sr2}=M_{sr} \\ M_{1a,2}+M_{1b,2}=M_{1a,3}+M_{1b,3}=M_s \end{cases} \quad (17)$$

It is also admitted [17] for from ITSC fault studies that:

$$\begin{cases} r^s_{1b}=k_{cc}r_s\,;\ l^s_{1b}=k_{cc}{}^2L^s \\ M^s=\dfrac{-L^s}{2};\ M^r=\dfrac{-L^r}{2} \\ M_{sr}=\sqrt{\left(L^sL^r\right)};\ M_{sr_1}=\left(1-k_{cc}\right)M^s;\ M_{sr_2}=k_{cc}M_{sr} \\ M_{1a,1b}=L^s\left(1-k_{cc}\right)k_{cc} \\ M_{1a,2}=M^s\left(1-k_{cc}\right);\ M_{1a,3}=M^s\left(1-k_{cc}\right) \\ M_{1b,2}=M^sk_{cc}\,;\ M_{1b,3}=M^sk_{cc} \end{cases} \quad (18)$$

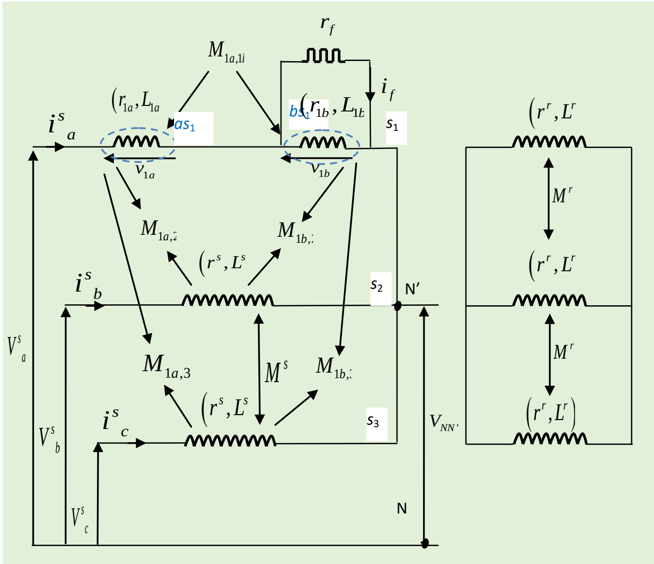

Fig. 6. Induction generator equivalent circuit under short-circuit fault.

Affected by ITSC fault, voltage equations become:

$$\begin{cases} \left[V^s{}_{abcf}\right]=\left[R^s{}_{abcf}\right]\left[i^s{}_{abc}\right]+\left[L^{ss}{}_{abcf}\right]\dfrac{d}{dt}\left[i^s{}_{abcf}\right] \\ \left[V^r{}_{abc}\right]=\left[0\right]=\left[R^r{}_{abc}\right]\left[i^r{}_{abc}\right]+\left[L^{rr}{}_{abc}\right]\dfrac{d}{dt}\left[i^r{}_{abc}\right] \end{cases}$$

$$+\ \begin{matrix} \dfrac{d}{dt}(\left[M^{sr}{}_{abcf}\right]\left[i^r{}_{abc}\right]) \\ \dfrac{d}{dt}(\left[M^{rs}{}_{abcf}\right]\left[i^s{}_{abcf}\right]) \end{matrix} \quad (19)$$

Where the new system vectors are:

$$[V^s{}_{abcf}]=\left[V^s{}_a \quad V^s{}_b \quad V^s{}_c \quad 0\right]^T;\ [V^r{}_{abc}]=\left[V^r{}_a \quad V^r{}_b \quad V^r{}_c\right]^T$$

$$[i^s{}_{abcf}]=\left[i^s{}_a \quad i^s{}_b \quad i^s{}_c \quad i_f\right]^T;\ [i^r{}_{abc}]=\left[i^r{}_a \quad i^r{}_b \quad i^r{}_c\right]^T$$

$[R^s{}_{abcf}]$ and $[R^r{}_{abc}]$ are the parametric resistance matrices written by:

$$\left[R^s{}_{abcf}\right]=\begin{bmatrix} r^s & 0 & 0 & -r^s_{1b} \\ 0 & r^s & 0 & 0 \\ 0 & 0 & r^s & 0 \\ r^s_{1b} & 0 & 0 & -(r^s_{1b}+r_f) \end{bmatrix} \left[R^r{}_{abc}\right]=\begin{bmatrix} r^r & 0 & 0 \\ 0 & r^r & 0 \\ 0 & 0 & r^r \end{bmatrix}$$

$[L^{ss}{}_{abcf}]$, $[L^{rr}{}_{abcf}]$ and $[M^{sr}{}_{abcf}(\theta)]$ are the parametric inductance matrices written by:

$$\left[L^{ss}{}_{abcf}\right]=\begin{bmatrix} L^s+l^s & M_{1a,2}+M_{1b,2} & M_{1a,3}+M_{1b,3} & -\left(L^s_{1b}+l^s_{1b}+M_{1a,1b}\right) \\ M_{1a,2}+M_{1b,2} & L^s+l^s & M^s & -M_{1b,2} \\ M_{1a,3}+M_{1b,3} & M^s & L^s+l^s & -M_{1b,3} \\ L^s_{1b}+l^s_{1b}+M_{1a,1b} & M_{1a,2} & M_{1a,3} & -\left(L^s_{1b}+l^s_{1b}\right) \end{bmatrix}$$

$$\left[L^{rr}{}_{abc}\right]=\begin{bmatrix} L^r+l^r & M^r & M^r \\ M^r & L^r+l^r & M^r \\ M^r & M^r & L^r+l^r \end{bmatrix} \quad \left[M^{rs}{}_{abcf}\right]=\left[M^{sr}{}_{abcf}\right]^T$$

$$\left[M^{sr}{}_{abcf}(\theta)\right]=\begin{bmatrix} M_{sr}\cos(\theta) & M_{sr}\cos(\theta+\frac{2\pi}{3}) & M_{sr}\cos(\theta-\frac{2\pi}{3}) \\ M_{sr}\cos(\theta-\frac{2\pi}{3}) & M_{sr}\cos(\theta) & M_{sr}\cos(\theta+\frac{2\pi}{3}) \\ M_{sr}\cos(\theta+\frac{2\pi}{3}) & M_{sr}\cos(\theta-\frac{2\pi}{3}) & M_{sr}\cos(\theta) \\ -M_{sr_2}\cos(\theta) & -M_{sr_2}\cos(\theta+\frac{2\pi}{3}) & -M_{sr_2}\cos(\theta-\frac{2\pi}{3}) \end{bmatrix}$$

4. Simulations Results of ITSC Fault Impact on the Wind Turbine System

Stator current, voltage and torque signals contain sufficient information about turn faults. Time-domain and frequency-domain signatures analysis are good tools for extracting ITSC fault impacts. The simulation are realized using the MATLAB/SIMULINK environment. To recognize the ITSC fault effect on the wind turbine system, we have applied a wind steady profile over a period of 2s.

A wind turbine system including a 14m radius-rotor turbine is used for simulations. The three bladed turbine is characterized by $J_{turbine}$=25 Kg.m², λ_{opt}=5 and C_{p_max}=0.44. The simulations are based on a 11 kW induction machine of 1450tr/min nominal speed, 4-poles, 50Hz frequency and 380/660V voltage. The machine parameters are given in Table. 1. The IG is characterized by stator turns number N^s=48, rotor turns number N^r=32, J_g=0.1 Kg.m², f=0.003 N.m.s, The load current i^s_0 = 4A and the rated current i^s_N=11.32A.

Table. 1. The induction generator parameters.

r^s (Ω)	r^r (Ω)	L^s (H)	L^r (H)	l^s (H)	l^r (H)
1.5	0.7	0.14	0.28	0.011	0.0075

In the initial phase, until t= 1.5s, no short-circuited turns are presented (healthy case). A ITSC fault is applied at t=1.5s (faulty case). The fault affects 30% of s_1-phase (30% ITSC turns characterized by k_{cc}=0.3). The diminution of the insulation resistance r_f in most materials from infinite toward zero is very fast, that's why r_f was fixed to 0Ω . The simulation results are presented in figures from Fig. 7 to Fig. 15 under fault appearing at the instant t=0.15s.

Fig. 7 shows that at t=1.5s, oscillations occur in the machine electromagnetic torque C_{em}. The supplied power to the grid P is disturbed (Fig. 8). Fig. 8 and Fig. 9 show the stator currents (i^s_a, i^s_b, i^s_c) and voltage (V^s_a, V^s_b, V^s_c) variation in the *(abc)* frame. Under healthy conditions, stator currents and voltages are balanced.

Once a ITSC fault occurs, an unbalance takes place at t=1.5s. The current i^s_a, circulating in the affected phase (s_1), increases significantly compared to other phase currents (i^s_b and i^s_c) (Fig.9). The stator voltage V^s_a, voltage of the affected phase (s_1), decreases significantly compared to other phase voltages (V^s_b and V^s_c) (Fig.10). It is also observed that the fluctuations rise in stator-side converter current i_{ch} (Fig.11). This indicates that the ITSC fault is influencing the whole system even with the presence of IRFOC loop.

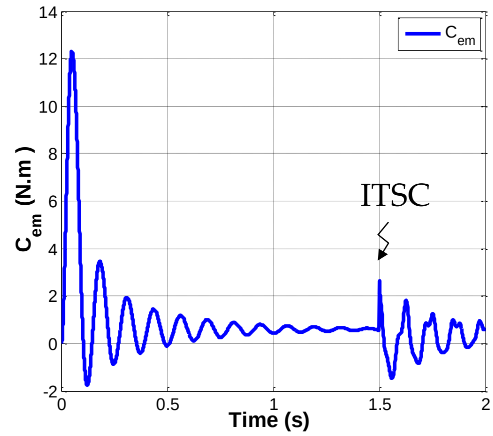

Fig. 7. Simulation result of torque C_{em} of wind turbine system IG with introduced ITSC fault of 30% of s_1-phase at t=1.5s.

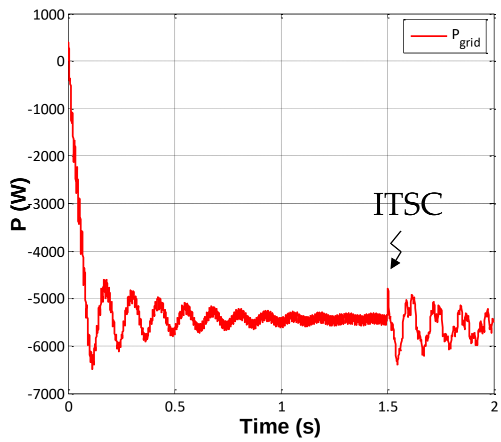

Fig. 8. Simulation result of supplied power P to the grid of wind turbine system IG with introduced ITSC fault of 30% of s_1-phase at t=1.5s.

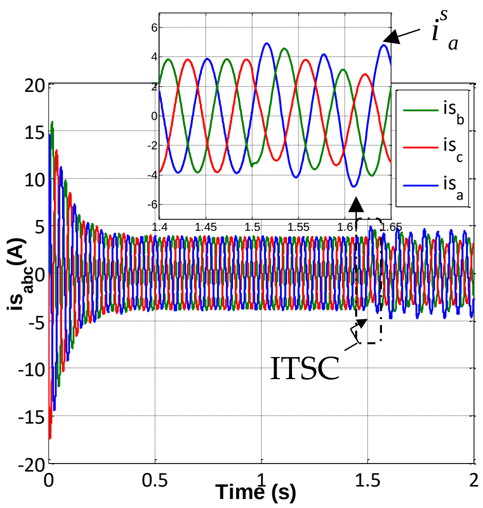

Fig. 9. Simulation result of three-phase stator currents i^s_{abc} and their zooms at t=1.5s of wind turbine system IG with ITSC fault of 30% of s_1-phase.

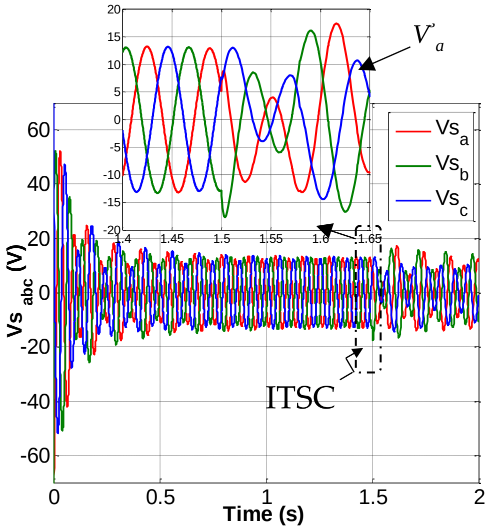

Fig. 10. Simulation result of three-phase stator voltages V^s_{abc} and their zooms at t=1.5s of wind turbine system IG with ITSC fault of 30% of s_1-phase.

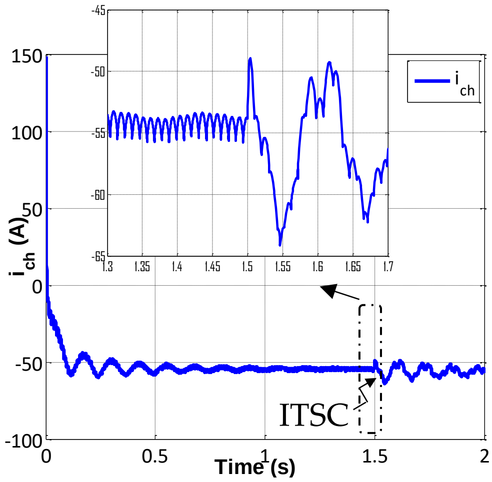

Fig. 11. Simulation result of stator-side converter current i_{ch} and its zoom at t t=1.5s of wind turbine IG with ITSC fault of 30% of s_1-phase.

In order to examine the IRFOC efficiency, controlled signals are presented under both healthy and faulty conditions. Fig. 12 presents the system mechanical speed Ω_{mec} and its reference Ω_{mec}^* under both healthy and faulty conditions. Rotor flux (φ_r) and its reference are plotted as shown by Fig. 13. Stator currents (i^s_d, i^s_q) and their references ($i^s_d{}^*$, $i^s_q{}^*$) in the (*dq*) frame are presented by respectively Fig. 14 and Fig. 15. It can be observed that the ITSC fault engenders important oscillations in estimated rotor flux and stator currents signals. Flux and currents carry on following their references but escorted by perturbations. These perturbations are also affecting the injected power to grid *P* signal stability. Although the system continues operating with the presented degraded performances, the quick detection and isolation of ITSC fault is extremely required once one turn is affected. In fact, the fault will spread so fast that the number of affected turns will increase. Therefore, the wind turbine must be stopped until the isolation of the fault in order to protect the equipment [19-21].

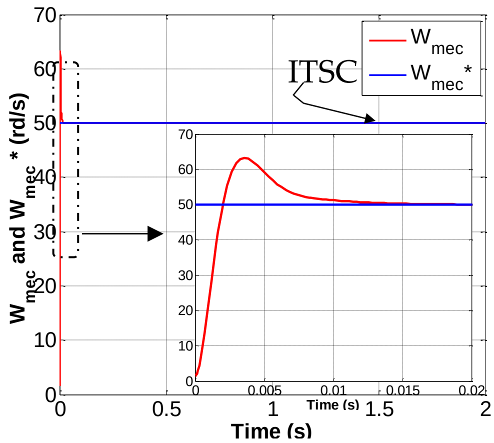

Fig. 12. Simulation result of mechanical speed Ω_{mec} and its reference Ω_{mec}^* using MPPT method and their zooms at t=0s of wind turbine IG with ITSC fault of 30% of s_1-phase.

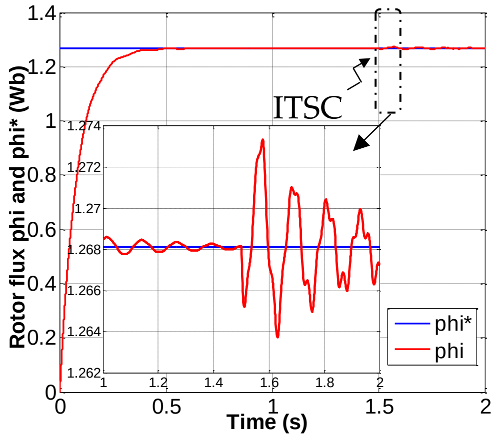

Fig. 13. Simulation result of estimated rotor flux φ_r and its reference φ_r^* using IRFOC method and their zooms at t=1.5s of wind turbine IG with ITSC fault of 30% of s_1-phase.

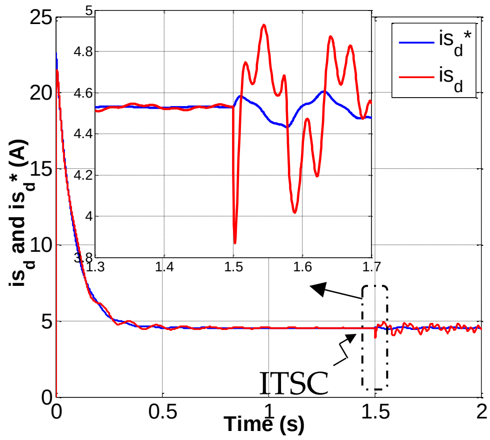

Fig. 14. Simulation result of current i^s_d and its reference $i^s_d{}^*$ using IRFOC method and their zooms at t=1.5s of wind turbine IG with ITSC fault of 30% of s_1-phase.

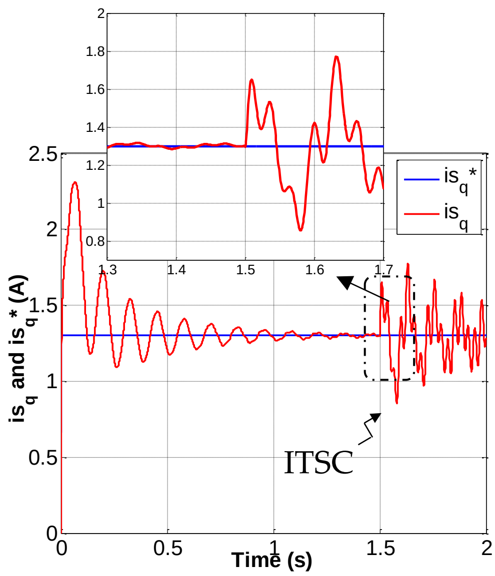

Fig. 15. Simulation result of current i^s_q and its reference $i^s_q{}^*$ using IRFOC method and their zooms at t=1.5s of wind turbine IG with ITSC fault of 30% of s_1-phase.

ITSC fault is so fast spread fault that the percentage of short-circuited turns can quickly increase. However, all experimental tests in the literature deal with only few short-circuited turns due to the risk of these tests (strong currents can damage the system). Thus, simulations are run under an introduced ITSC fault with a higher number of short-circuited turns (50% of the s_1-phase are affected) in order to examine the fault impact on the system if it is forced to continue operating after the fault occurrence. Fig. 16 and Fig. 17 show the machine torque C_{em} and the power P injected to the grid under faulty conditions at t=1.5s. Fig. 18 shows the current of the stator-side converter i_{ch}. The IRFOC controlled current i^s_q and its reference $i^s_q{}^*$ are presented in Fig. 19. It can be observed that the system is out of service after one second due to the significant increase in these signals at t=1.5s. It can be deducted that if the system is forced to continue operating, it will operate up to 50% of one phase are affected with dangerous outputs. Hence, IRFOC scheme has to be replaced by a fault tolerant control technique once ITSC fault is detected. The fault tolerant scheme must compensate the signals fluctuations and the currents increase caused by the fault and ensure the continuation of the operation in spite of ITSC fault presence [22-29].

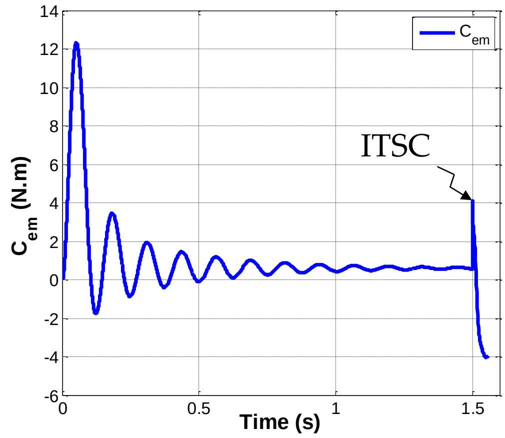

Fig. 16. Simulation result of torque C_{em} of wind turbine system IG with introduced ITSC fault of 50% of s_1-phase at t=1.5s.

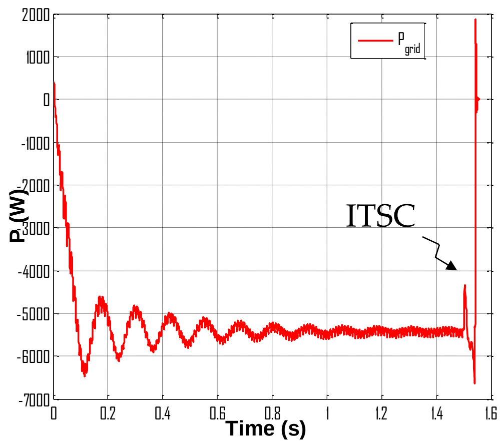

Fig. 17. Simulation result of supplied power P to the grid of wind turbine system IG with introduced ITSC fault of 50% of s_1-phase at t=1.5s.

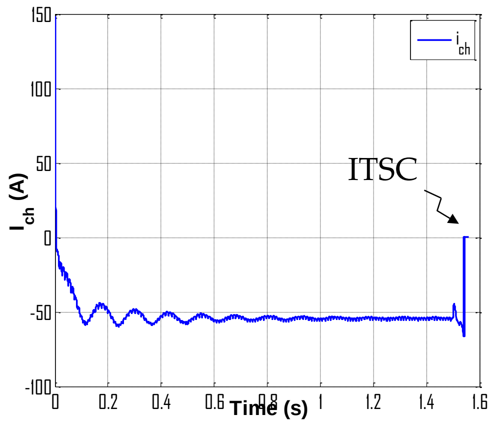

Fig. 18. Simulation result of stator-side converter current i_{ch} of wind turbine system IG with introduced ITSC fault of 50% of s_1-phase at t=1.5s.

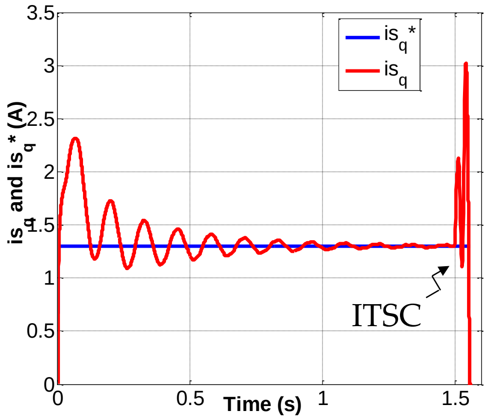

Fig. 19. Simulation result of current i^s_q with its reference $i^s_q{}^*$ using IRFOC method of wind turbine system IG with introduced ITSC fault of 50% of s_1-phase at t=1.5s.

5. Conclusions

Inter-turn short-circuit faults are typically the final consequence of the incessant aging of winding insulations of machines caused by transient overvoltage or vibration. In this context, this paper studied ITSC fault affecting IG of grid connected wind turbine systems. The presented results illustrate that once ITSC fault appears, the induction generator currents are disturbed causing perturbations in the stator-side converter input voltages and output currents. Hence, the supplied power to the grid is directly fluctuated which engender an instability of the grid connection. Furthermore, the thermal impact of the generated fault current, circulating through the damaged turns, increasingly destroys the insulation of the affected and adjacent turns. The slot insulation or insulation of the other two phases of the IG can be also affected because of the fast spread of ITSC fault, which can engender a catastrophic phase-to-phase or even to phase-to-ground failures. The simulation results demonstrate that if no efficient fault detection and isolation scheme is executed within a few seconds, the localized ITSC fault can progress to catastrophic destructions of the generator and the converter of the wind turbine system.

Acknowledgements

This research project was supported by the both Tunisian and French Ministries of High Education and Scientific Research.

References

[1] JM. Carrasco, LG. Franquelo, JT. Bialasiewicz, E. Galván, RC. PortilloGuisado, MM. Prats and N. Moreno-Alfonso ,"Power-Electronic Systems for the Grid Integration of Renewable Energy Sources: A Survey," IEEE Transactions on industrial electronics, VOL. 53, NO. 4, August 2006.

[2] YS. Hameed, YS. Hong, YM. Cho, SH. Ahn, and CK. Song, "Condition monitoring and fault detection of wind turbine and related algorithms: A review," Renewable and sustainable energy reviews, Volume 13, Issue 1, Pages 1–39, January 2009.

[3] T. Sellami, H. Berriri, S. Jelassi and M.F. Mimouni, "Sliding Mode Observer-Based Fault-Detection of Inter-Turn Short-Circuit in Induction Motor," 14th international conference on Sciences and Techniques of Automatic control & computer engineering - STA'2013, 978-1-4799-2954-2/13/$31.00 ©2013 IEEE.

[4] P.C.M. Lamim Filh, R. Pederiva and J.N. Brito, "Review Detection of stator winding faults in induction machines using flux and vibration analysis," Mechanical Systems and Signal Processing , Elsevier 2014.

[5] RR. Schoen, BK. Lin, TG. Habetler, JH. Schlag and S. Farag, "An unsupervised, on-line system for induction motor fault detection using stator current monitoring," IEEE Transactions on Industry Applications 1995.

[6] CC. Ciang, L. Jung-Ryul and B. Hyung-Joon, "Structural health monitoring for a wind turbine system: a review of damage detection methods," Measurement Science and Technology, October 2008.

[7] AG. Abo-Khalil and L. Dong-Choon, "MPPT control of wind generation systems based on estimated wind speed using SVR," IEEE Transactions on Industrial Electronics 55.3 : 1489-1490, 2008.

[8] S. Krim, S. Gdaim, A. Mtibaa and MF. Mimouni, "FPGA Contribution in Photovoltaic Pumping Systems: Models of MPPT and DTC-SVM Algorithms," International Journal of Renewable Energy Research (IJRER), 6(3), 866-879, 2016.

[9] H. Tajima and H. Yoichi, "Speed sensorless field-orientation control of the induction machine," IEEE Transactions on Industry Applications 29.1: 175-180, 1993.

[10] TA. Tapia, G. Tapia, J.X. Ostolaza, and JR. Sáenz, "Modeling and Control of a Wind Turbine Driven Doubly Fed Induction Generator," IEEE Transactions on energy conversion, vol. 18, NO. 2, JUNE 2003.

[11] S. Toumi, S. Benelghali, M. Trabelsi, E. Elbouchikhi, Y. Amirat, M. Benbouzid and MF. Mimouni, "Modeling and Simulation of a PMSG-based Marine Current Turbine System under Faulty Rectifier Conditions," Electric Power Components and Systems, 45(7), 715-725, 2017.

[12] T. Sellami, H. Berriri, S. Jelassi, AM. Darcherif and M.F. Mimouni, "3D Finite Volume model for free and forced vibrations computation in on-shore wind turbines," In Information and Digital Technologies (IDT), 2017 International Conference on (pp. 104-108). IEEE. 2017.

[13] T. Sellami, H. Berriri, AM. Darcherif, S. Jelassi and M.F. Mimouni, "Modal and harmonic analysis of three-dimensional wind turbine models," Wind Engineering, 40(6), 518-527, 2016.

[14] GM. Joksimovic and J. Penman, "The detection of inter-turn short circuits in the stator windings of operating motors," IEEE Transactions on Industrial Electronics, 47(5), 1078-1084, 2000.

[15] F. Grouz, L. Sbita and M. Boussak, "PSO based Multiple and Simultaneous Inter-Turn Short Circuit Faults

Diagnosis of PMSG for Wind Turbine Applications," International Journal Transactions on Systems, Signals and Devices, Issues on Power Electrical Systems, 2017.

[16] E. Artigao, A. Honrubia-Escribano and E. Gomez-Lazaro, "Current signature analysis to monitor DFIG wind turbine generators: A case study," Renewable Energy 2017.

[17] A. Gandhi, T, Corrigan and L. Parsa, "Recent advances in modeling and online detection of stator interturn faults in electrical motors," IEEE Transactions on Industrial Electronics, 58(5), 1564-1575, 2011.

[18] T. Sellami, H. Berriri, S. Jelassi, AM. Darcherif and M.F. Mimouni, "Impact of Inter-Turn Short-Circuit Fault on Wind Turbine Driven Squirrel-Cage Induction Generator Systems," In Conférence Internationale en Sciences et Technologies Electriques au Maghreb CISTEM 2014, November 2014.

[19] Y. Krim, S. Krim and MF. Mimouni, "Control of a Wind Farm Connected to the Grid at a Frequency and Variable Voltage," International Journal of Renewable Energy Research (IJRER), 6(3), 747-758, 2016.

[20] M. Riera-Guasp, JA. Antonino-Daviu and GA. Capolino, "Advances in electrical machine, power electronic, and drive condition monitoring and fault detection: state of the art," IEEE Transactions on Industrial Electronics, 62(3), 1746-1759, 2015.

[21] A. Sallam, RA. Hamdy, MMZ. Moustafa and A. Hossam-Eldin, "New measurement technique for modular multilevel converter with IGBT open-circuit failure detection and tolerance control for three-level submodule," In Renewable Energy Research and Applications (ICRERA), 2016 IEEE International Conference on (pp. 452-457). IEEE, November 2016.

[22] KH. Ahmed and GP. Adam, "Fault tolerant multi-kW DC transformer structure for wind farms," In Renewable Energy Research and Applications (ICRERA), 2016 IEEE International Conference on (pp. 820-825). IEEE, November 2016.

[23] AO. Di Tommaso, F. Genduso, R. Miceli and GR. Galluzzo, "A review of multiple faults diagnosis methods in voltage source inverters," In Renewable Energy Research and Applications (ICRERA), 2015 International Conference on (pp. 1376-1381). IEEE, November 2015.

[24] VF. Pires, D. Foito and TG. Amaral, "Fault detection and diagnosis in a PV grid-connected T-type three level inverter," In Renewable Energy Research and Applications (ICRERA), 2015 International Conference on (pp. 933-937). IEEE, November 2015.

[25] KH. Ahmed and GP. Adam, "Fault tolerant multi-kW DC transformer structure for wind farms," In Renewable Energy Research and Applications (ICRERA), 2016 IEEE International Conference on (pp. 820-825). IEEE, November 2016.

[26] ME. Emna, K. Adel and MF. Mimouni, "The wind energy conversion system using PMSG controlled by vector control and SMC strategies," International Journal of Renewable Energy Research (IJRER), 3(1), 41-50, 2013.

[27] T. Sellami, H. Berriri, S. Jelassi, A. M Darcherif and M.F. Mimouni, "Short-Circuit Fault Tolerant Control of a Wind Turbine Driven Induction Generator Based on Sliding Mode Observers ," Energies, 10(10), 1611, 2017.

[28] T. Sellami, H. Berriri, S. Jelassi, A. M Darcherif and M.F. Mimouni, "Sliding Mode Observers-based Fault Detection and Isolation for Wind Turbine-Driven Induction Generator," International Journal of Power Electroni-cs and Drive Systems (IJPEDS), 8(3), 2017.

[29] T. Sellami, S. Jelassi, H. Berriri, A. M Darcherif and M.F. Mimouni, "Validation expérimentale d'un modèle numérique 3D pour la conception des éoliennes sous contraintes vibratoires: Plateforme TREVISE," In 5ème colloque Analyse Vibratoire Expérimentale (AVE), November 2017.